5700 *Biochemistry* **2009,** *48,* 5700–5707
DOI: 10.1021/bi900366p

BIOCHEMISTRY
including biophysical chemistry & molecular biology
Article

Effects of Zn^{2+}, Ca^{2+}, and Mg^{2+} on the Structure of Zn_7Metallothionein-3: Evidence for an Additional Zinc Binding Site[†]

Gabriele Meloni,[‡] Thomas Polanski,[‡] Oliver Braun, and Milan Vašák*

Department of Biochemistry, University of Zurich, Winterthurerstrasse 190, CH-8057 Zurich, Switzerland
[‡] These authors contributed equally to this work

Received March 4, 2009; Revised Manuscript Received May 6, 2009

ABSTRACT: Human metallothionein-3 (Zn_7MT-3), an intra- and extracellularly occurring metalloprotein, is highly expressed in the brain, where it plays an important role in the homeostasis of the essential metal ions Cu^+ and Zn^{2+}. Like other mammalian metallothioneins (MT-1 and -2), the protein contains a $M^{II}_3(CysS)_9$ and a $M^{II}_4(CysS)_{11}$ cluster localized in two independent protein domains linked by a flexible hinge region. However, there is a substantially increased number of acidic residues in MT-3 (11 residues) compared with MT-2 (four residues) which may act as binding ligands for additional metal ions. In this study, the binding of Zn^{2+}, Ca^{2+}, and Mg^{2+} to human Zn_7MT-3 and its mutant lacking an acidic hexapeptide insert, Zn_7MT-$3^{\Delta 55-60}$, was investigated and compared with the binding of Zn_7MT-2. By using spectroscopic and spectrometric techniques, we demonstrate that one additional Zn^{2+} binds with an apparent binding constant (K_{app}) of ~100 μM to Zn_7MT-3 and Zn_7MT-$3^{\Delta 55-60}$, but not to Zn_7MT-2. The changes in spectroscopic features of metal−thiolate clusters and gel filtration behavior reveal that the formation of Zn_8MT-3 is immediate and is accompanied by a decrease in the Stokes radius (R_s). The changes in the R_s suggest a mutual approach of both protein domains. The fast binding of Zn^{2+} is followed by a slow time-dependent protein dimerization. The binding of Zn^{2+} to Zn_7MT-3 is specific as in the presence of Ca^{2+} and Mg^{2+} only an alteration of the R_s of Zn_7MT-3 at substantially higher concentrations was observed. The significance of these findings for the biological role of MT-3 is discussed.

The brain has the highest content of zinc of all organs with an average total zinc concentration estimated to be approximately 150 μM (*1*). This trace element plays structural, catalytic, or regulatory roles in numerous enzymes and other proteins (*2*). Apart from its importance in protein complexes, the zinc ion is closely involved in intracellular signaling and neurotransmission. In the mammalian brain, 10−15% of the total Zn^{2+} is localized in presynaptic vesicles of zinc-enriched neurons (ZEN),[1] a subclass of glutamatergic neurons (*3*). ZEN are present in many regions of the central nervous system (CNS) and are especially abundant in the hippocampus. The best established function for released Zn^{2+} into the synaptic cleft is the modulation of the glutamate and GABA receptors on postsynaptic cells (*4*). Cellular zinc uptake is controlled by a family of membranous zinc transporter proteins called ZIPs, whereas the zinc transporters ZnTs, which belong to the cation diffusion facilitator family (CDF), mediate zinc efflux (*5*). While in the synaptic vesicles of ZEN an approximately millimolar concentration of chelatable Zn^{2+} was found, that in the cytosol is in the subnanomolar range. Low intracellular free Zn^{2+} concentrations in neurons are maintained by the action of cytosolic metal binding proteins, the most abundant of which is metallothionein-3 (MT-3). This metalloprotein reversibly binds seven Zn^{2+} ions with high affinity through an array of 20 Cys residues. Zn_7MT-3, also termed the neuronal growth inhibitory factor (GIF), occurs intra- and extracellularly and shows neuroinhibitory activity in vitro that distinguishes it from the widely expressed MT-1 and MT-2 isoforms (*6*, *7*). Thus, MT-3, but not MT-1 or -2, antagonizes the ability of Alzheimer's disease (AD) brain extract to stimulate survival and neuritic sprouting of cultured neurons (*6*, *8*). This extracellular bioactivity led to the hypothesis that Zn_7MT-3 may be involved in pathogenic processes leading to AD. The observation that Zn_7MT-3 protects the neuronal cells from the toxic effect of amyloid-β (Aβ), by abolishing the production of reactive oxygen species (ROS) and related cellular toxicity caused by the redox cycling of Aβ-Cu(II), strongly supports its protective role in AD (*9*, *10*).

[†]This work was supported by Swiss National Science Foundation Grant 3100A0-111884 to M.V.

*To whom correspondence should be addressed. Telephone: +41-44-635-55-52. Fax: +41-44-635-59-05. E-mail: mvasak@bioc.uzh.ch.

[1]Abbreviations: ZEN, zinc-enriched neurons; CNS, central nervous system; GABA, γ-aminobutyric acid; ZIP, Zrt- and Irt-like proteins; ZnT, zinc transporters; CDF, cation diffusion facilitator; MT, metallothionein; GIF, growth inhibitory factor; AD, Alzheimer's disease; Aβ, amyloid-β; ROS, reactive oxygen species; SDS, sodium dodecyl sulfate; ESI-MS, electrospray ionization mass spectrometry; DTP, 2,2′-dithiopyridine; EDTA, ethylenediaminetetraacetic acid; CD, circular dichroism; Tris, tris(hydroxymethyl)aminomethane; SEC, size exclusion chromatography; NMR, nuclear magnetic resonance; LMCT, ligand-to-metal charge transfer.

Published on Web 05/08/2009

Table 1: Spectroscopic and Hydrodynamic Properties of Zn_7MT-3, Zn_7MT-$3^{\Delta 55-60}$, and Zn_7MT-2 in the Presence of Zn^{2+}

	circular dichroism (CD) experiments		size exclusion chromatography (SEC) experiments			
protein	$\Delta[\theta]_{197}$ (%)	K_{app}[a] ($\times 10^{-3}$ M)	R_S (Å)	$R_{S,min}$ (Å)	ΔR_S[a] (%)	K_{app}[a] ($\times 10^{-3}$ M)
Zn_7MT-3	14.4 ± 0.5	0.13 ± 0.03	23.7	21.8	8.0 ± 0.7	0.13 ± 0.04
Zn_7MT-$3^{\Delta 55-60}$	10.9 ± 3.0	0.15 ± 0.09	22.4	20.9	7.9 ± 0.6	0.09 ± 0.02
Zn_7MT-2	−	−	20.5	20.1	(1.8 ± 0.8)	−

[a] Errors from nonlinear regression analysis using a one-site binding model.

The studies of MT-3 and zinc transporter 3 (ZnT3) knockout mice revealed that ZnT3, which concentrates Zn^{2+} in presynaptic vesicles, and MT-3 function in the same pathway (*11*). From these studies, an important role for intracellular Zn_7MT-3 in the recycling of Zn^{2+} has been suggested (*12*). The in vitro demonstration of the direct interaction of Zn_7MT-3 with Rab3A, a small GTPase involved in the regulation of the synaptic vesicle cycle, further supports this role (*13*, *14*). Zn^{2+} is released from presynaptic neurons in a Ca^{2+}- and impulse-dependent fashion, reaching a concentration in the synaptic cleft of up to ~300 μM (*15*). Whether the extracellularly occurring Zn_7MT-3 plays a role in controlling zinc concentrations and zinc-dependent processes in the extracellular space is currently not known.

Structural studies conducted on well-defined MT-3 metalloforms containing 7 molar equiv of either Zn^{2+} or Cd^{2+} ions have revealed that $M_7^{II}MT$-3, like other mammalian metallothioneins, contains two metal−thiolate clusters localized in two independent protein domains: a three-metal cluster $[M_3^{II}(CysS)_9]$ in the N-terminal β-domain and a four-metal cluster $[M_4^{II}(CysS)_{11}]$ in the C-terminal α-domain (*16*−*18*). ESI-MS studies have shown that in contrast to MT-1 and -2, the formation of both metal−thiolate clusters in MT-3 is noncooperative (*19*). However, compared to MT-1 and -2 isoforms, the primary structure of MT-3 contains a substantially increased number of acidic residues, i.e., 11 in MT-3 vs 4 in MT-2, which may act as binding ligands for additional metal ions.

In this work, the metal binding capacity of MT-3 and structural features developing upon binding of more than 7 molar equiv of divalent metal ions have been studied. The binding of Zn^{2+}, Ca^{2+}, and Mg^{2+} to human Zn_7MT-3 and its mutant lacking the acidic hexapetide insert Zn_7MT-$3^{\Delta 55-60}$ was investigated and compared with that of the well-chracterized isoform Zn_7MT-2. We demonstrate that in contrast to Zn_7MT-2, both Zn_7MT-3 forms bind specifically one additional Zn^{2+}, forming Zn_8MT-3. Zinc binding induces marked and immediate structural changes in the monomeric Zn_8MT-3 form, which are followed by a slow time-dependent dimerization process. While the presence of Ca^{2+} and Mg^{2+} resulted in the alteration of Zn_7MT-3 structure, no evidence of a specific binding site for both metal ions was obtained. The implications of this study for the function of MT-3 are discussed.

EXPERIMENTAL PROCEDURES

Reagents. Media for protein expression were purchased from BD (Becton, Dickinson and Co., Sparks, MD). All standard reagents were of the highest purity available from common commercial sources. All solutions were rendered metal-free by being treated with Chelex 100 (Bio-Rad) to prevent metal contamination.

Protein Expression and Purification. A deletion mutant of human MT-3, human MT-$3^{\Delta 55-60}$, lacking amino acids ^{55}EAAEAE^{60} was generated by Primm (Milan, Italy). For recombinant protein expression, a pET-3d (Novagen) plasmid encoding human MT-3, human MT-$3^{\Delta 55-60}$, or the human MT-2 sequence was used. The expression in *Escherichia coli* strain BL21 (DE3) pLys and the purification were performed as previously described (*16*). The metal-free protein (apoprotein) was generated according to the method of Vašák (*20*). The purity and correctness of the masses of the expressed proteins were confirmed by SDS−PAGE and ESI-MS analysis, respectively (*21*). Fully Zn^{2+}- and Cd^{2+}-loaded protein forms were prepared by metal reconstitution as described previously (*20*). The metal-to-protein ratios were determined by measuring the absorbance of the metal-free protein (thionein) at 220 nm in 0.1 M HCl using the extinction coefficients for human MT-3 (ε_{220} = 53000 M^{-1} cm^{-1}), human MT-$3^{\Delta 55-60}$ (ε_{220} = 49000 M^{-1} cm^{-1}), and human MT-2 (ε_{220} = 48200 M^{-1} cm^{-1}) and the metal content determined by flame atomic absorption spectroscopy (SpectrAA-110, Varian Inc.). Cysteine-to-protein ratios were determined via photometric quantification of the sulfhydryl groups (CysSH) upon their reaction with 2,2′-dithiopyridine (DTP) in 0.2 M sodium acetate and 1 mM EDTA (pH 4.0) using an ε_{343} of 7600 M^{-1} cm^{-1} (*22*). In all cases, a metal-to-protein ratio of 7.0 ± 0.3 and a CysSH-to-protein ratio of 20 ± 2 were obtained.

UV−Vis and Circular Dichroism (CD) Spectroscopy. The UV−Vis absorption measurements of Zn_7MT-3 (6 μM) in the presence of 0−500 μM $ZnCl_2$ were performed on a Cary 3 (Varian) spectrophotometer. A Jasco spectropolarimeter (model J-810) was used for CD measurements. The concentrations of Zn_7MT-3, Zn_7MT-$3^{\Delta 55-60}$, Zn_7MT-2, and Cd_7MT-3 were between 45 and 65 μM in 25 mM Tris-HCl and 50 mM NaCl (pH 8.0). The CD spectra were recorded in the range between 260 and 195 nm in the presence of 0, 0.1, 0.25, 0.5, and 1 mM $ZnCl_2$ and are expressed as molar ellipticity [θ], in units of deg $dmol^{-1}$ cm^2. The final spectra were smoothed using the FFT algorithm of Origin version 7.5 (OriginLab Corp., Northampton, MA). Zinc-induced changes in the molar ellipticity at 197 nm ($\Delta[\theta]_{197}$) were plotted versus the Zn^{2+} concentration and analyzed by nonlinear regression analysis using a one-site binding model (Origin version 7.5). From the fit, the apparent binding constant (K_{app}) and the maximal changes in the molar ellipticity under saturating conditions were obtained (Table 1).

Analysis of the Stokes Radius. The Stokes radius for MTs in the presence of increasing concentrations of Zn^{2+} was determined using analytical size exclusion chromatography (SEC) experiments at room temperature. A Superdex 75, 10/300 GL column (GE Healthcare) was equilibrated with 25 mM Tris-HCl and 50 mM NaCl (pH 8.0) and eluted with a flow rate of 1 mL/min. The column was calibrated using cytochrome *c* (12400 Da), carbonic anhydrase (29000 Da), and bovine serum albumin (66000 Da) as molecular mass markers (MW-GF-70,

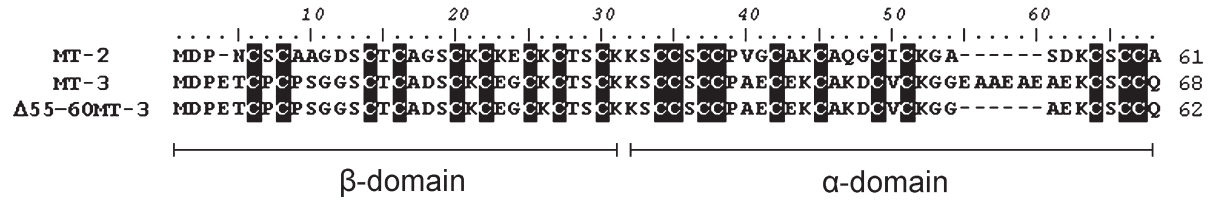

FIGURE 1: Sequence alignment of human MT-2, human MT-3, and the mutant MT-$3^{\Delta 55-60}$ generated using CLUSTALW. The conserved cysteines are shown in bold. The numbering is that of the human MT-3 sequence.

Sigma). The distribution coefficient (K_{av}) for each protein sample was calculated according to the relationship $K_{av} = V_e - V_0/V_t - V_0$, where V_e is the elution volume of the protein, V_t is the total column volume, and V_0 is the void volume. The Stokes radius (R_S) was calculated form a linear plot of $(-\log K_{av})^{1/2}$ versus the R_S of the marker proteins (bovine serum albumin, R_S = 37.0 Å; carbonic anhydrase, R_S = 24.0 Å; and cytochrome *c*, R_S = 19.0 Å) according to Laurent and Killander (*23*). The changes in R_S were plotted versus the Zn^{2+} concentration and analyzed by a nonlinear regression analysis using a one-site binding model. From the fit, the apparent binding constants (K_{app}) were obtained (Table 1).

ESI-MS Analysis. For nano-ESI-MS measurements, 300 μL of 60 μM Zn_7MT-3 and Cd_7MT-3 in 25 mM Tris-HCl and 50 mM NaCl (pH 8.0) were incubated with 200 μM $ZnCl_2$ and 60 μM $CdCl_2$, respectively. Prior to MS, the buffer was exchanged using a Microcon YM3 ultrafiltration device (Millipore Corp.) by three washing cycles (3 × 500 μL) with 10 mM 4-ethylmorpholine (pH 7.2) to remove NaCl and the sample concentrated to a final concentration of ~200 μM. For ESI-MS analysis, protein samples were diluted into a 5 mM ammonium acetate/acetonitrile/methanol/water mixture (10:12.5:37.5:50, pH 7.5−8.0) and infused through a fused silica capillary (inside diameter of 75 μm) at a flow rate of 0.5 μL/min into a nano-ESI-MS Q-TOF Ultima API mass sprectrometer (Micromass). Electrospray PicoTIPS (inside diameter of 30 μm) were obtained from New Objective (Woburn, MA). MS spectra were recorded in a positive mode at a capillary exit voltage of 2.1 kV, a cone voltage of 50 V, and an RF lens energy of 50 V. Mass spectra were deconvoluted using MaxEnt-1 (Micromass).

^{113}Cd NMR Measurements. Protein samples were prepared in 25 mM Tris-HCl and 50 mM NaCl (pH 8.0) and concentrated to 3 mM using a polyether sulfone membrane (cutoff of 5 kDa) (Millipore Corp.) prior to NMR measurements. The ^{113}Cd NMR spectra of $^{113}Cd_7$MT-3 were recorded on a Bruker DRX-500 spectrometer using inverse-gated broadband proton decoupling to account for possible negative ^{113}Cd−^{1}H NOE. ^{113}Cd spectra were acquired over a 30000 Hz spectral width using an acquisition time of 0.8 s and a relaxation delay of 0.3 s (*16*). All NMR samples contained 10% ^2H_2O for the field-frequency lock and were measured in 5 mm NMR tubes at 323 K. The ^{113}Cd chemical shifts are reported in parts per million relative to the ^{113}Cd resonance of 0.1 M $Cd(ClO_4)_2$ in ^2H_2O.

RESULTS

Circular Dichroism and Electronic Absorption Studies of the Interaction of Zn^{2+} with Zn_7MT-3, Zn_7MT-$3^{\Delta 55-60}$, and Zn_7MT-2. To explore the effect of additional metal ions bound to Zn_7MT-3 on the protein structure and to learn more about the specificity of metal binding, we have performed circular dichroism (CD) experiments in the presence of increasing concentrations of Zn^{2+}, Ca^{2+}, and Mg^{2+}. Since MT-3 is the only

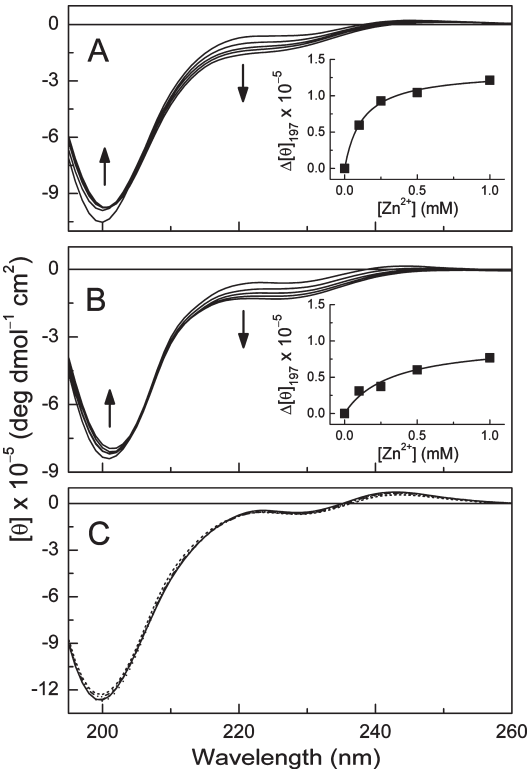

FIGURE 2: Effect of Zn^{2+} on the circular dichroism (CD) spectra of Zn_7MT isoforms: (A) Zn_7MT-3, (B) Zn_7MT-$3^{\Delta 55-60}$, and (C) Zn_7MT-2. The proteins were titrated with 0, 0.1, 0.25, 0.5, and 1 mM $ZnCl_2$ in 25 mM Tris-HCl and 50 mM NaCl (pH 8.0). Arrows indicate the effect of increasing Zn^{2+} concentrations. Insets show changes in the molar ellipticity [θ] at 197 nm plotted vs Zn^{2+} concentration. The data were fitted by a nonlinear regression analysis using a one-site binding model.

MT isoform containing a glutamate-rich hexapeptide insert in the C-terminal α-domain (Figure 1), the CD features of Zn_7MT-3 were compared with those of the mutant Zn_7MT-$3^{\Delta 55-60}$, lacking the hexapeptide insert, and the structurally well-characterized human Zn_7MT-2 (*24*).

The presented CD spectra of Zn_7MTs in Figure 2A−C are characterized by a biphasic CD profile with bands at (+)247 and (−)228 nm and a crossover point at 239 nm, originating from an excitonic splitting of the first CysS−Zn(II) ligand-to-metal charge transfer (LMCT) band at 235 nm (*16*). A strong CD band at (−)200 nm is dominated by the peptide backbone transitions. The CD titration of Zn_7MT-3 and Zn_7MT-$3^{\Delta 55-60}$ with increasing Zn^{2+} concentrations (0−1 mM) revealed, besides an intensity decrease of the (−)200 nm CD band, significant changes also between 210 and 260 nm consistent with a perturbation of the metal−thiolate cluster structure. Specifically, while the (−)223 nm shoulder experienced an increase in intensity, the intensity of the (+)245 nm CD band in the low-energy region decreased and underwent a gradual 5 nm red shift paralleled by a

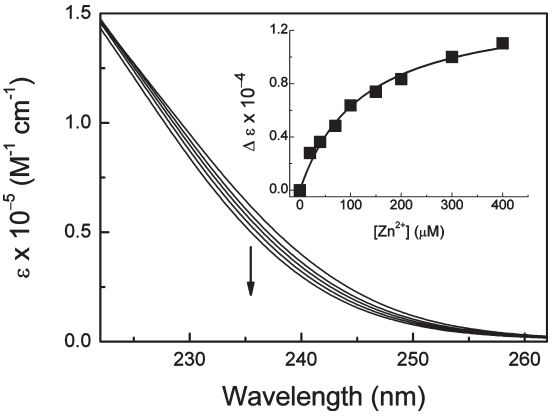

FIGURE 3: Effect of Zn^{2+} on the electronic absorption spectrum of Zn_7MT-3. The protein was titrated with 0, 30, 50, 70, 100, 150, 200, 250, 300, 350, and 400 μM $ZnCl_2$ in 25 mM Tris-HCl and 50 mM NaCl (pH 8.0). The arrow indicates the effect of increasing concentrations of Zn^{2+}. The inset shows changes in the extinction coefficient ($\Delta\varepsilon$) at 235 nm plotted vs Zn^{2+} concentration. The data were fitted by a nonlinear regression analysis using the one-site binding model.

4 nm red shift of the crossover point from 238 to 242 nm. The occurrence of an isodichroic point at ~205 nm with an increasing Zn^{2+} concentration suggests that two structurally different ZnMT-3 forms are concomitantly present in solution. In contrast, only minor changes were observed in the CD spectrum of Zn_7MT-2 upon Zn^{2+} addition (Figure 2C). To assess the maximal changes in the secondary structure of Zn_7MT-3 and Zn_7MT-3$^{\Delta55-60}$ under saturating conditions, the changes in molar ellipticity at 197 nm ($\Delta[\theta]_{197}$) were plotted versus the Zn^{2+} concentration (insets in Figure 2A,B). From a nonlinear regression analysis using a one-site binding model (see below), an apparent dissociation constant (K_{app}) of $(0.13 \pm 0.03) \times 10^{-3}$ M was calculated for Zn^{2+} binding to Zn_7MT-3 and a value of $(0.15 \pm 0.09) \times 10^{-3}$ M for binding to Zn_7MT-3$^{\Delta55-60}$ (Table 1). The similarity between both values indicates that the acidic hexapeptide insert is not essential for the binding of additional Zn^{2+}.

The effect of addition of Zn^{2+} on the absorption spectrum of Zn_7MT-3 was also examined (Figure 3). Because of the absence of aromatic residues and histidine in MTs, the absorption spectra of all Zn_7MTs are characterized by a metal-induced shoulder around 235 nm, originating from CysS−Zn(II) LMCT transitions. With increasing Zn^{2+} concentrations, the absorption shoulder of Zn_7MT-3 decreased in intensity. This effect most likely originates from the perturbation of excitonic interactions within the clusters seen in the CD spectra. A similar effect has been observed upon the perturbation of excitonic interactions in α-helical proteins and model peptides (*25*). The curve analysis of the changes in absorbance at 235 nm ($\Delta[\varepsilon]_{235}$) versus the Zn^{2+} concentration revealed a K_{app} of $(0.12 \pm 0.02) \times 10^{-3}$ M (Figure 3, inset). Analogous analysis of the corresponding changes in molar ellipticity of Zn_7MT-3 at 235 nm resulted in a closely similar K_{app} of $(0.11 \pm 0.01) \times 10^{-3}$ M (Figure 2A). Overall, the effect of Zn^{2+} addition on the LMCT bands in the absorption and CD spectra of Zn_7MT-3 is paralleled by that observed on peptide backbone transitions in the corresponding CD spectrum. The close correspondence of the determined K_{app} indicates that both effects relate to Zn^{2+} binding to Zn_7MT-3 (Figure 2A). Moreover, while a similar behavior was also seen with Zn_7MT-3$^{\Delta55-60}$, the spectrum of Zn_7MT-2 was unaffected by Zn^{2+} addition (Figure 2C).

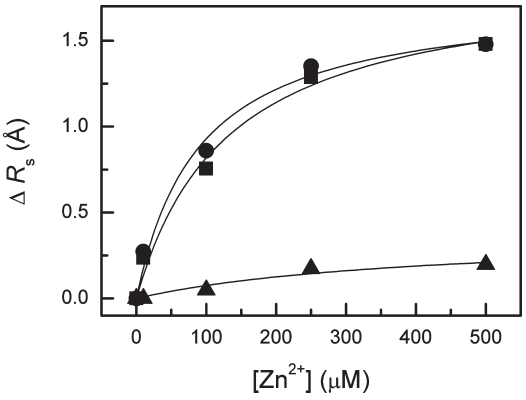

FIGURE 4: Changes in the Stokes radius (ΔR_S) of Zn_7MT-3 (■), Zn_7MT-3$^{\Delta55-60}$ (●), and Zn_7MT-2 (▲) determined by size exclusion chromatography in the absence and presence of 10, 100, 250, and 500 μM $ZnCl_2$ in elution buffer [25 mM Tris-HCl and 50 mM NaCl (pH 8.0)].

Effect of Zn^{2+} on the Hydrodynamic Properties of Zn_7MT-3, Zn_7MT-3$^{\Delta55-60}$, and Zn_7MT-2. To asses whether the observed changes in the secondary structure also lead to changes in the tertiary structure, the hydrodynamic properties of Zn_7MT-3, Zn_7MT-3$^{\Delta55-60}$, and Zn_7MT-2 in the presence and absence of increasing Zn^{2+} concentrations in the elution buffer were investigated by analytical size exclusion chromatography (SEC). In the absence of Zn^{2+} in the elution buffer, monomeric Zn_7MT-3, Zn_7MT-3$^{\Delta55-60}$, and Zn_7MT-2 elute from the column with apparent molecular masses (M_{app}) of 25600, 21900, and 17300 Da, respectively. The increased apparent molecular masses of these 7−8 kDa proteins reflect a prolate ellipsoid shape of mammalian MTs (*26*). The corresponding Stokes radii (R_S) were calculated according to Laurent and Killander's equation (*23*). In the presence of Zn^{2+} (0−500 μM), Zn_7MT-3 and Zn_7MT-3$^{\Delta55-60}$ exhibited a concentration-dependent decrease in the R_S (Figure 4) with maximal changes of 8.0 and 7.9%, respectively (Table 1). In contrast, only minor (< 2%) changes in R_S were observed with Zn_7MT-2. These R_S values reflect the maximal changes in ΔM_{app} of 5200 Da for Zn_7MT-3, 3700 Da for Zn_7MT-3$^{\Delta55-60}$, and < 1000 Da for Zn_7MT-2. Using a one-metal binding site model and assuming that the measured changes in Stokes radii are directly proportional to metal binding, the K_{app} values for Zn_7MT-3 and Zn_7MT-3$^{\Delta55-60}$ of 0.13×10^{-3} and 0.09×10^{-3} M, respectively, were determined by nonlinear regression analysis. These K_{app} values are similar to those obtained in the corresponding CD and absorption studies, suggesting that the methods describe the same binding process (Table 1).

ESI-MS Analysis of Zn_8MT-3. To further investigate the metal binding stoichiometry of Zn_7MT-3 with additional Zn^{2+} bound, we performed ESI-MS analysis at pH 7.5. In view of the K_{app} value of ~100 μM, the sample of 60 μM Zn_7MT-3 in 25 mM Tris-HCl and 50 mM NaCl (pH 8.0) was mixed with 200 μM $ZnCl_2$. This was followed by three washing steps to remove NaCl, and the sample was then concentrated to a final concentration of ~200 μM and analyzed. As depicted in Figure 5, besides the mass peak of Zn_7MT-3 (7368.6 Da), an additional mass peak with a mass difference of 62.8 Da corresponding to one Zn^{2+} (calculated Δm of 63.4 Da) was observed. This signifies that the Zn_7MT-3 form is capable of binding one additional metal ion forming Zn_8MT-3. The presence of Zn_7MT-3 in the MS spectra of Zn^{2+} derivatives reflects the instability of Zn_8MT-3 during the MS analysis. Thus, in our MS experiments, we could not confirm

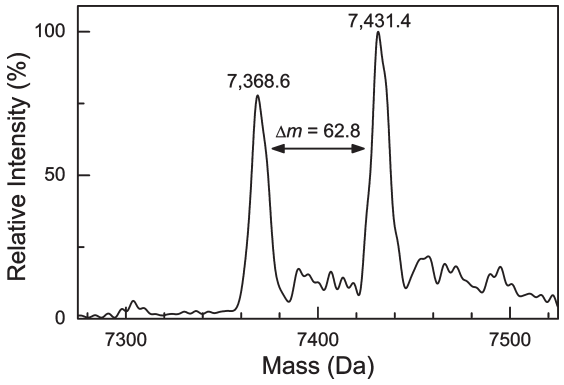

FIGURE 5: Deconvoluted nano-ESI-MS spectrum of Zn_8MT-3 at pH 7.5. For details of sample preparation, see Experimental Procedures.

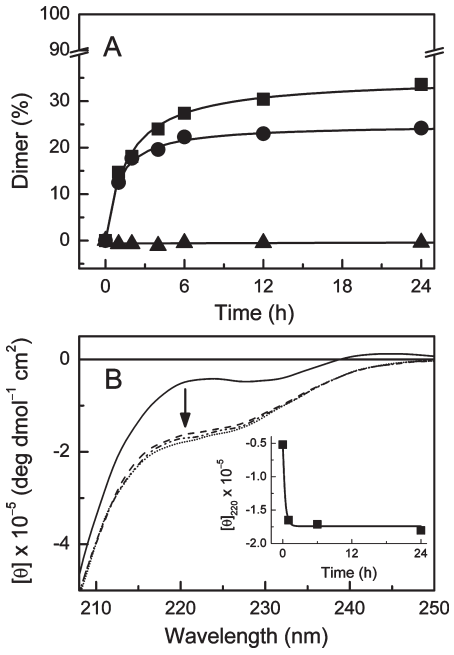

FIGURE 6: (A) Kinetics of dimer formation of Zn_7MT isoforms monitored by size exclusion chromatography in the presence of 1 mM $ZnCl_2$ in elution buffer. The samples of ZnMT-2 (▲), ZnMT-$3^{\Delta 55-60}$ (●), and ZnMT-3 (■), were incubated with 1 mM $ZnCl_2$. (B) The circular dichroism (CD) spectra of ZnMT-3 recorded after 0, 1, 6, and 24 h upon addition of 1 mM $ZnCl_2$. Conditions: 25 mM Tris-HCl and 50 mM NaCl (pH 8.0). The arrow indicates the CD changes with increasing incubation time.

the formation of MT-3 to Zn^{2+} stoichiometries higher than 8 as previously reported (*19*). We ascribe these differences in the ESI-MS spectra to different conditions used in sample preparations.

Kinetics of Zn^{2+}-Dependent Dimerization of Zn_7MT-3 and Zn_7MT-$3^{\Delta 55-60}$. During the determination of the R_S in the presence of Zn^{2+}, we observed after a 24 h incubation with Zn^{2+} that besides monomeric forms of Zn_8MT-3 and Zn_8MT-$3^{\Delta 55-60}$ dimers (M_{app} ~ 38000 Da) and to a minor extent higher oligomers (< 3%) were also formed (data not shown). To further investigate the kinetic properties of this dimerization process, the 50 μM samples of Zn_7MT-3, Zn_7MT-$3^{\Delta 55-60}$, and Zn_7MT-2 were incubated in the presence of 1 mM Zn^{2+}, and at various incubation times, aliquots were subjected to SEC and eluted with buffer containing 1 mM Zn^{2+}. The presented time courses in Figure 6A reveal the maximal formation of ~30% dimers for Zn_8MT-3 and ~25% for Zn_8MT-$3^{\Delta 55-60}$ after incubation for 12 h, with a half-maximal dimer formation reached already after incubation for ~2 h. However, no dimer formation was observed for Zn_7MT-2. Rechromatography of the isolated dimer fractions again yielded a monomeric and dimeric protein, indicating its nonoxidative nature. The absence of intermolecular disulfides was further confirmed by ESI-MS analysis of dimers at low pH (pH 3). The generated apoproteins revealed only the mass peak of the monomer (data not shown). As no dimers were formed after incubation of Zn_7MT-3, Zn_7MT-$3^{\Delta 55-60}$, and Zn_7MT-2 for 24 h in the absence of Zn^{2+} or in the presence of 50 mM Mg^{2+} (see below), the presence of Zn^{2+} is critical for the dimerization process (Figure 1 of the Supporting Information). To assess the effect of protein dimerization on the cluster structure of Zn_7MT-3, we have recorded CD spectra immediately following Zn^{2+} addition and after sample incubation for 1, 3, 6, and 12 h. As seen in Figure 6B, the changes in the cluster structure of Zn_7MT-3 are completed immediately after the addition of Zn^{2+}. The absence of further CD changes with prolonged incubation times suggests that in dimers no further major perturbation of the cluster structure occurs. Since our attempts to characterize the dimeric form by ESI-MS failed, the metal content of dimers is not known. Nevertheless, the data suggest that a rapid structural rearrangement leading to the formation of Zn_8MT-3 results in a decrease in the R_S and that this is followed by a slow protein dimerization.

^{113}Cd NMR Studies of CdMT-3 Dimers. We have used the CdMT-3 derivative to learn more about the nature of MT-3 dimers. In the past, the isostructural substitution of Zn^{2+} ions in MTs with Cd^{2+} provided a wealth of information regarding the structure of these proteins (*27*, *28*). At first, to aid our ^{113}Cd NMR studies, we examined whether the binding of additional Cd^{2+} ions to Cd_7MT-3 also forms Cd_8MT-3. The ESI-MS spectrum of Cd_8MT-3, generated in a manner similar to that of Zn_8MT-3, showed the predominant mass peak of 7810.5 Da, clearly indicating that Cd_8MT-3 is formed (Figure 2 of the Supporting Information). As the binding of extra Zn^{2+} significantly perturbed the cluster structure in Zn_7MT-3, we studied the effect of both Zn^{2+} and Cd^{2+} ions on the CD spectrum of Cd_7MT-3 (Figure 3 of the Supporting Information). In Cd_7MT-3, the spectral contribution of peptide transitions to LMCT bands is negligible, due to the red shift of the CysS−Cd^{2+} LMCT bands of ~20 nm compared to those in the Zn_7MT-3 form. The CD spectrum of Cd_7MT-3 shows, besides a strong CD band of peptide backbone transitions at (−)200 nm, a biphasic CD profile with extrema at (−)237 and (+)257 nm and a crossover point at 246 nm. Like those of Zn_7MT-3, the low-energy CD features in Cd_7MT-3 originate from excitonic splitting of the first CysS−Cd^{2+} LMCT band. The successive addition of Zn^{2+} or Cd^{2+} to Cd_7MT-3 resulted in immediate changes in the cluster structure characterized by the development of two isodichroic points at ~240 and ~257 nm observed with both metal ions. Their presence suggests that the Me^{II}_7MT-3 and Me^{II}_8MT-3 forms are concomitantly present in solution. These results further suggest that the effect of both metal ions on the structure of Cd_7MT-3, leading to the formation of Me^{II}_8MT-3, is similar. In the case of Cd^{2+}, the immediate saturation of the additional metal binding site in Cd_7MT-3 occurred at ~100 μM, indicating a higher affinity for Cd^{2+} than for Zn^{2+} where a 1 mM concentration was required. The incubation of Cd_7MT-3 with Zn^{2+} and Cd^{2+} for 48 h gave rise to dimer formation (40% with Zn^{2+} and 80% with Cd^{2+}). Next, we carried out ^{113}Cd NMR experiments on Cd_7MT-3 monomers and CdMT-3 dimers (Figure 7). The ^{113}Cd NMR spectrum of $^{113}Cd_7$MT-3 presented in Figure 7A compares well with that published. As previously shown, the strong ^{113}Cd

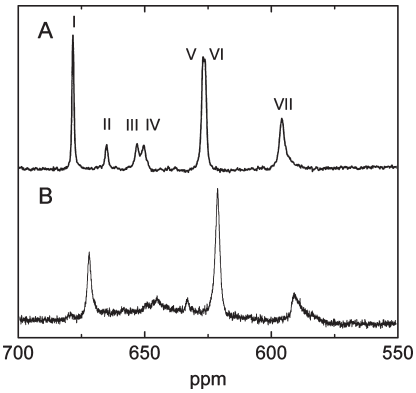

FIGURE 7: ^{113}Cd NMR spectra (110.9 MHz) of human (A) Cd_7MT-3 and (B) CdMT-3 dimers in 25 mM Tris-HCl and 50 mM NaCl (pH 8.0, 323 K). Labeled ^{113}Cd resonances I, V, VI, and VII originate from the Cd_4 cluster in the α-domain, whereas resonances II, III, and IV originate from the Cd_3 cluster in the β-domain of Cd_7MT-3.

resonances (I, V, VI, and VII) originate from the Cd_4 cluster and the three weak resonances (II, III, and IV) originate from the Cd_3 cluster (*16*). The characteristic features of this spectrum are a large apparent line width of all resonances (150−350 Hz), the absence of homonuclear ^{113}Cd−^{113}Cd couplings, and a markedly reduced and temperature-independent intensity (20%) of the resonances of the Cd_3 cluster. These features have been interpreted in terms of dynamic processes acting on two different NMR time scales: fast exchange processes among conformational cluster substates occurring in both clusters and additional slow exchange processes among configurational cluster substates in the Cd_3 cluster (*16*). The latter exchange processes allowed only the structure of the α-domain of $^{113}Cd_7$MT-3 to be determined by NMR (*18*).

The dimeric sample for NMR measurements was generated by overnight incubation of $^{113}Cd_7$MT-3 (0.1 mM) with the 6-fold excess of $^{113}Cd^{2+}$ followed by the sample concentration reaching ~3 mM. The gel filtration chromatographic check of this sample, conducted as described above for Zn^{2+} dimers, revealed that in the CdMT-3 sample ~80% of dimers were present. The ^{113}Cd NMR spectrum of mainly dimeric ^{113}CdMT-3 is shown in Figure 7B. Besides the ^{113}Cd resonances shown, no additional resonances were observed in the spectral range between −100 and 900 ppm. In this spectrum, the ^{113}Cd resonances of the Cd_4 cluster appear to be less affected, showing only a small high-field shift in their chemical shift position (~6 ppm). However, the weak ^{113}Cd resonances occurring at different chemical shift positions compared with the monomeric form most likely originate from the Cd_3 cluster resonances in dimers. Whether a high-field shoulder at resonance VII comes from the altered Cd_3 cluster or from the perturbation of this site is not clear. We ascribe the absence of ^{113}Cd resonances of the additional weakly bound metal ion(s) to a chemical exchange.

Circular Dichroism Studies of the Interaction of Ca^{2+} and Mg^{2+} with Zn_7MT-3, Zn_7MT-3$^{\Delta 55-60}$, and Zn_7MT-2. In view of the large number of acidic residues in MT-3, the interaction of Zn_7MT-3, Zn_7MT-3$^{\Delta 55-60}$, and, for comparison, Zn_7MT-2 with Ca^{2+} and Mg^{2+}, which often bind specifically to these residues, was also investigated. The studies were conducted using Ca^{2+} and Mg^{2+} concentrations between 1 and 50 mM. However, no effect of these metal ions on the CD spectra of all Zn_7MTs was seen. The representative CD spectrum of Zn_7MT-3, showing the effect of increasing Mg^{2+} concentrations, is presented in Figure 8A.

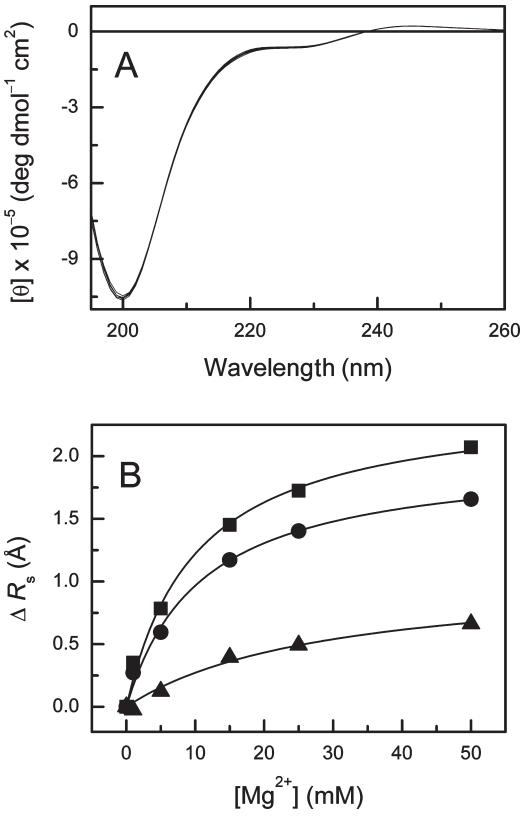

FIGURE 8: (A) Effect of increasing Mg^{2+} concentrations (between 0 and 50 mM) on the circular dichroism (CD) spectrum of Zn_7MT-3. (B) Changes in the Stokes radius (ΔR_S) of Zn_7MT-3 (■), Zn_7MT-3$^{\Delta 55-60}$ (●), and Zn_7MT-2 (▲) as a function of increasing Mg^{2+} concentration in elution buffer determined by size exclusion chromatography.

Effect of Ca^{2+} and Mg^{2+} on the Hydrodynamic Properties of Zn_7MT-3, Zn_7MT-3$^{\Delta 55-60}$, and Zn_7MT-2. In marked contrast to the CD studies, the presence of Ca^{2+} and Mg^{2+} between 1 and 50 mM affected the hydrodynamic properties of the studied Zn_7MTs to a different extent. Since the effect of both metals on the Stokes radii was found to be similar and occurred at rather high concentrations, only the effect of more physiologically relevant Mg^{2+} is presented (Figure 8B). Furthermore, the close similarity of the R_S values for these proteins obtained in 50 and 100 mM NaCl indicates that the observed effect originates mainly from the presence of these divalent metal ions. Although the dependence of the R_S versus Mg^{2+} concentration resembles that obtained for Zn_7MT-3 and Zn_7MT-3$^{\Delta 55-60}$ upon Zn^{2+} binding (Figure 4), the changes in the R_S with Mg^{2+} occurred at 100-fold higher concentrations. The results show that the presence of millimolar Mg^{2+} concentrations induced substantial changes in the apparent Stokes radii (Figure 8B). Thus, whereas in the CD studies no evidence of changes in the protein structure in the presence of Ca^{2+} and Mg^{2+} was obtained, the R_S values of all Zn_7MTs, including Zn_7MT-2, were affected to a different extent by both metal ions. Consequently, the effect of Zn^{2+} on the structure of Zn_7MTs differs from that of Ca^{2+} and Mg^{2+}. Overall, these results support a specific effect of Zn^{2+} on the structure of Zn_7MT-3 and Zn_7MT-3$^{\Delta 55-60}$.

DISCUSSION

In these studies, we demonstrate that Zn_7MT-3 can specifically bind one additional Zn^{2+} with an apparent binding constant (K_{app}) of ~100 μM. The immediate formation of Zn_8MT-3 is

accompanied by the perturbation of the cluster structure and the reduction of the Stokes radius (Table 1), features consistent with the mutual approach of both protein domains which are linked by a flexible hinge region. As both Zn_7MT-3 and the Zn_7MT-$3^{\Delta 55-60}$ mutant exhibited the same behavior, the acidic hexapeptide insert (E^{55}AAEAE^{60}) is not essential for the formation of Zn_8MT-3. In marked contrast, the addition of Zn^{2+} ions was without effect on the structure of well-characterized Zn_7MT-2, suggesting that the formation of Zn_8MT-3 is specific to this isoform. The reductions of Stokes radii of Zn_7MT-3, Zn_7MT-$3^{\Delta 55-60}$, and Zn_7MT-2 were also seen with Ca^{2+} and Mg^{2+}, but at substantially higher concentrations compared with that of Zn^{2+} (~100 times). This and the absence of changes in the corresponding CD spectra suggest that the effect of Zn^{2+} is specific and differs from that of Ca^{2+} and Mg^{2+}. The influence of Ca^{2+} and Mg^{2+} on Stokes radii of all Zn_7MTs studied appears to be complex and may include changes in protein hydration shell as well as a weak binding of Ca^{2+} and Mg^{2+} to protein carboxylates, reducing the degree of electrostatic repulsion between both protein domains. In this context, it should be noted that the charge difference between the α-domains of Zn_7MT-3 and Zn_7MT-2 is −5.0 and that between their β-domains is −2.0.

A prolonged incubation of MT-3 with Zn^{2+}, but not with Ca^{2+} or Mg^{2+}, results in a slow protein dimerization characterized by an increased apparent molecular mass and the absence of changes in the CD spectra. The noncovalent nature of dimers was confirmed by ESI-MS analysis of the apoprotein. The CD studies of the dimerization process using the Cd_7MT-3 form revealed that both Zn^{2+} and Cd^{2+} cause a similar immediate perturbation of the cluster structure, due to the formation of Me^{II}_8MT-3, and that no further CD changes occur during the slow protein dimerization. This suggests that the initial formation of Me^{II}_8MT-3 generates a protein surface needed for its dimerization. Although the instability of the dimer under ESI-MS conditions prevented the determination of its metal content, the involvement of additional metal ions in the dimer formation and stabilization cannot be ruled out. The ^{113}Cd NMR studies of CdMT-3 dimers were conducted on the sample containing mainly the dimeric form (~80%). The ^{113}Cd NMR spectrum of dimers shows, besides almost unperturbed resonances of the Cd_4 cluster, additional weak resonances occurring at a different chemical shift position compared with that of Cd_7MT-3. We assigned the latter ^{113}Cd resonances to the Cd_3 cluster in dimers. Thus, it would appear that the mutual approach of both protein domains and the protein dimerization mainly affect the more flexible Cd_3 cluster. In view of the substantially increased number of acidic residues in MT-3 (11 residues) compared with MT-2 (4 residues), we suggest that the carboxylate donor ligands present on the surface of both domains in MT-3 participate in binding of the additional Zn^{2+} to Zn_7MT-3. The absence of ^{113}Cd resonances in the spectral range of oxygen or oxygen/nitrogen donor ligands between −100 and 400 ppm in CdMT-3 dimers is due most likely to chemical exchange. However, the participation of original terminal thiolate ligand(s) of the Cd_3 cluster in metal binding cannot be ruled out.

Biological implications of these studies should also be discussed. As Zn_7MT-3 occurs intra- and extracellularly, the protein is exposed to different concentrations of Zn^{2+}, Ca^{2+}, and Mg^{2+}. Zn_7MT-3 is mainly expressed in ZEN (*29*). In the cytosol of these neurons, the free zinc concentration is in subnanomolar range and thus without effect on the structure of Zn_7MT-3. However, in the extracellular space, the free zinc concentration reaches up to 300 μM during synaptic signaling (*15*). Under these conditions, the binding of Zn^{2+} to excreted Zn_7MT-3 would generate the Zn_8MT-3 form. A reversible switch between the Zn_7- and Zn_8-MT-3 forms, depending on the fluctuation in zinc concentrations during synaptic neurotransmission, may be important as a zinc buffer or for an interaction with binding partner(s). In contrast to Zn^{2+}, the interaction of Ca^{2+} and Mg^{2+} with Zn_7MT-3 is unspecific and occurs at substantially higher concentrations of these metal ions. Whereas the extracellular concentration of Ca^{2+} and Mg^{2+} is ~1−2.5 mM, a total cytosolic concentration of Ca^{2+} is 100 μM and the intracellular concentration of Mg^{2+} is 10−20 mM. The former metal ion, through an increase in its free cytosolic concentration from 0.1 to 0.5 μM, acts as a second messenger (*30*). Therefore, only the intracellular Mg^{2+} concentration may influence the structure of Zn_7MT-3. Cell culture studies using cultured cortical neurons showed that the major part of intracellular Mg^{2+} is bound to low-molecular mass components such as ATP and that the free Mg^{2+} concentration upon neuronal stimulation can increase up to 10−12 mM (*31*). In view of these studies, Mg^{2+} would exert a significant effect on the structure of Zn_7MT-3 under conditions of neuronal stimulation. Thus, the structure of intra- and extracellularly occurring MT-3 will be influenced in a different way by free Mg^{2+} and Zn^{2+} levels. These structural changes may be important for the function of this protein in different environments.

ACKNOWLEDGMENT

We thank Dr. Thomas Fox (Institute of Inorganic Chemistry, University of Zurich) for the ^{113}Cd NMR measurements and Dr. Serge Chesnov (Functional Genomics Center Zurich, University of Zurich) for the ESI-MS measurements.

SUPPORTING INFORMATION AVAILABLE

Three figures show the kinetics of dimer formation of ZnMT-3 and the ESI-MS and circular dichroism spectra of Cd_8MT-3. This material is available free of charge via the Internet at http://pubs.acs.org.

REFERENCES

1. Takeda, A. (2000) Movement of zinc and its functional significance in the brain. *Brain Res. Brain Res. Rev. 34*, 137–148.
2. Vallee, B. L., and Falchuk, K. H. (1993) The biochemical basis of zinc physiology. *Physiol. Rev. 73*, 79–118.
3. Frederickson, C. J. (1989) Neurobiology of zinc and zinc-containing neurons. *Int. Rev. Neurobiol. 31*, 145–238.
4. Frederickson, C. J., Koh, J. Y., and Bush, A. I. (2005) The neurobiology of zinc in health and disease. *Nat. Rev. Neurosci. 6*, 449–462.
5. Liuzzi, J. P., and Cousins, R. J. (2004) Mammalian zinc transporters. *Annu. Rev. Nutr. 24*, 151–172.
6. Uchida, Y., Takio, K., Titani, K., Ihara, Y., and Tomonaga, M. (1991) The growth inhibitory factor that is deficient in the Alzheimer's disease brain is a 68 amino acid metallothionein-like protein. *Neuron 7*, 337–347.
7. Uchida, Y., Gomi, F., Masumizu, T., and Miura, Y. (2002) Growth inhibitory factor prevents neurite extension and death of cortical neurons caused by high oxygen exposure through hydroxyl radical scavenging. *J. Biol. Chem. 277*, 32353–32359.
8. Sewell, A. K., Jensen, L. T., Erickson, J. C., Palmiter, R. D., and Winge, D. R. (1995) Bioactivity of metallothionein-3 correlates with its novel β domain sequence rather than metal binding properties. *Biochemistry 34*, 4740–4747.
9. Irie, Y., and Keung, W. M. (2001) Metallothionein-III antagonizes the neurotoxic and neurotrophic effects of amyloid β peptides. *Biochem. Biophys. Res. Commun. 282*, 416–420.
10. Meloni, G., Sonois, V., Delaine, T., Guilloreau, L., Gillet, A., Teissie, J., Faller, P., and Vašák, M. (2008) Metal swap between

Zn_7-metallothionein-3 and amyloid-β-Cu protects against amyloid-β toxicity. *Nat. Chem. Biol. 4*, 366–372.
11. Cole, T. B., Robbins, C. A., Wenzel, H. J., Schwartzkroin, P. A., and Palmiter, R. D. (2000) Seizures and neuronal damage in mice lacking vesicular zinc. *Epilepsy Res. 39*, 153–169.
12. Aschner, M., Cherian, M. G., Klaassen, C. D., Palmiter, R. D., Erickson, J. C., and Bush, A. I. (1997) Metallothioneins in brain: The role in physiology and pathology. *Toxicol. Appl. Pharmacol. 142*, 229–242.
13. Kang, Q. H., Chen, Q. L., Ren, H. W., and Ru, B. G. (2001) Growth inhibitory factor (GIF) directly interacts with G-protein Rab3a. *Prog. Biochem. Biophys. 28*, 880–884.
14. Knipp, M., Meloni, G., Roschitzki, B., and Vašák, M. (2005) Zn_7metallothionein-3 and the synaptic vesicle cycle: Interaction of metallothionein-3 with the small GTPase Rab3A. *Biochemistry 44*, 3159–3165.
15. Assaf, S. Y., and Chung, S. H. (1984) Release of endogenous Zn^{2+} from brain tissue during activity. *Nature 308*, 734–736.
16. Faller, P., Hasler, D. W., Zerbe, O., Klauser, S., Winge, D. R., and Vašák, M. (1999) Evidence for a dynamic structure of human neuronal growth inhibitory factor and for major rearrangements of its metal-thiolate clusters. *Biochemistry 38*, 10158–10167.
17. Oz, G., Zangger, K., and Armitage, I. M. (2001) Three-dimensional structure and dynamics of a brain specific growth inhibitory factor: Metallothionein-3. *Biochemistry 40*, 11433–11441.
18. Wang, H., Zhang, Q., Cai, B., Li, H., Sze, K. H., Huang, Z. X., Wu, H. M., and Sun, H. (2006) Solution structure and dynamics of human metallothionein-3 (MT-3). *FEBS Lett. 580*, 795–800.
19. Palumaa, P., Eriste, E., Njunkova, O., Pokras, L., Jornvall, H., and Sillard, R. (2002) Brain-specific metallothionein-3 has higher metal-binding capacity than ubiquitous metallothioneins and binds metals noncooperatively. *Biochemistry 41*, 6158–6163.
20. Vašák, M. (1991) Metal removal and substitution in vertebrate and invertebrate metallothioneins. *Methods Enzymol. 205*, 452–458.
21. Meloni, G., Knipp, M., and Vašák, M. (2005) Detection of neuronal growth inhibitory factor (metallothionein-3) in polyacrylamide gels and by Western blot analysis. *J. Biochem. Biophys. Methods 64*, 76–81.
22. Pedersen, A. O., and Jacobsen, J. (1980) Reactivity of the thiol group in human and bovine albumin at pH 3−9, as measured by exchange with 2,2′-dithiodipyridine. *Eur. J. Biochem. 106*, 291–295.
23. Laurent, T. C., and Killander, J. (1964) Theory of gel filtration and its experimental verification. *J. Chromatogr. 14*, 317–330.
24. Messerle, B. A., Schaffer, A., Vašák, M., Kagi, J. H., and Wuthrich, K. (1992) Comparison of the solution conformations of human [Zn7]-metallothionein-2 and [Cd7]-metallothionein-2 using nuclear magnetic resonance spectroscopy. *J. Mol. Biol. 225*, 433–443.
25. Woody, R. W., and Koslowski, A. (2002) Recent developments in the electronic spectroscopy of amides and α-helical polypeptides. *Biophys. Chem. 101−102*, 535–551.
26. Vašák, M., Berger, C., and Kagi, J. H. (1984) Dynamic structure of metallothionein. *FEBS Lett. 168*, 174–178.
27. Vašák, M. (1998) Application of ^{113}Cd NMR to metallothioneins. *Biodegradation 9*, 501–512.
28. Oz, G., Pountney, D. L., and Armitage, I. M. (1998) NMR spectroscopic studies of $I = 1/2$ metal ions in biological systems. *Biochem. Cell Biol. 76*, 223–234.
29. Masters, B. A., Quaife, C. J., Erickson, J. C., Kelly, E. J., Froelick, G. J., Zambrowicz, B. P., Brinster, R. L., and Palmiter, R. D. (1994) Metallothionein III is expressed in neurons that sequester zinc in synaptic vesicles. *J. Neurosci. 14*, 5844–5857.
30. Pozzo-Miller, L. D., Pivovarova, N. B., Connor, J. A., Reese, T. S., and Andrews, S. B. (1999) Correlated measurements of free and total intracellular calcium concentration in central nervous system neurons. *Microsc. Res. Tech. 46*, 370–379.
31. Brocard, J. B., Rajdev, S., and Reynolds, I. J. (1993) Glutamate-induced increases in intracellular free Mg^{2+} in cultured cortical neurons. *Neuron 11*, 751–757.